Global Water Scarcity Assessment Incorporating Green Water in Crop Production

Wenfeng Liu, Xingcai Liu, Hong Yang, Philippe Ciais, Yoshihide Wada

AGU ADVANCING EARTH AND SPACE SCIENCE

Water Resources Research

RESEARCH ARTICLE
10.1029/2020WR028570

Global Water Scarcity Assessment Incorporating Green Water in Crop Production

Wenfeng Liu[1], Xingcai Liu[2,3], Hong Yang[2,4], Philippe Ciais[5], and Yoshihide Wada[6]

[1]Center for Agricultural Water Research in China, College of Water Resources and Civil Engineering, China Agricultural University, Beijing, China, [2]Eawag, Swiss Federal Institute of Aquatic Science and Technology, Duebendorf, Switzerland, [3]Key Laboratory of Water Cycle and Related Land Surface Processes, Institute of Geographic Sciences and Natural Resources Research, Chinese Academy of Sciences, Beijing, China, [4]Department of Environmental Sciences, MGU, University of Basel, Basel, Switzerland, [5]Laboratoire des Sciences du Climat et de l'Environnement, LSCE/IPSL, CEA-CNRS-UVSQ, Université Paris-Saclay, Gif-sur-Yvette, France, [6]International Institute for Applied Systems Analysis, Laxenburg, Austria

Abstract Over the past decades, water scarcity has become prevalent in many regions of the world. Previous water scarcity assessments largely considered "blue water" (surface and groundwater) and overlooked "green water" (soil moisture), despite its key role in supporting crop production. Moreover, the long-term evolution of water scarcity remains unclear. Here, we propose an agricultural water scarcity index (WSI_{AW}) that explicitly combines green and blue water. The WSI_{AW} measures the degree to which both green and blue water availabilities can satisfy the agricultural water requirement. The WSI_{AW} can directly indicate water scarcity in both rainfed and irrigated areas, which cannot be captured by the blue water scarcity index alone. Using the WSI_{AW}, we assessed the evolution of water scarcity across regions of the world during 1971–2010 at a spatial resolution of 0.5 arc degree. We found that 22% of the 228 river basins with a WSI_{AW} of >1 presented a much broader geographical coverage compared with estimates of water scarcity based on blue water only (8% of total basins). The WSI_{AW} also exhibited a clear trend of increasing severity over the study period, particularly in major agricultural regions. Expanding cropland and increasing/competing water withdrawals by other sectors were the main reasons for the intensification of water scarcity, which was pronounced in some Asian and African river basins. The proposed WSI_{AW} can be applied to different regions with various scales and is important for addressing global water scarcity issues.

Key Points:

- We propose a new agricultural water scarcity index (WSI_{AW}) by explicitly incorporating green and blue water for crop production
- WSI_{AW} indicated severe water scarcity over a much broader geographical coverage compared with water scarcity based on blue water only
- WSI_{AW} exhibited an increasing trend in many regions, mainly due to expanding cropland and increasing water withdrawals by other sectors

Supporting Information:

Supporting Information may be found in the online version of this article.

Correspondence to:

W. Liu,
wenfeng.liu@cau.edu.cn;
wenfengliu@vip.sina.com

Citation:

Liu, W., Liu, X., Yang, H., Ciais, P., & Wada, Y. (2022). Global water scarcity assessment incorporating green water in crop production. *Water Resources Research*, *58*, e2020WR028570. https://doi.org/10.1029/2020WR028570

Received 6 AUG 2020
Accepted 19 DEC 2021

Author Contributions:

Conceptualization: Wenfeng Liu, Hong Yang
Funding acquisition: Wenfeng Liu, Hong Yang
Investigation: Wenfeng Liu, Xingcai Liu
Methodology: Wenfeng Liu, Xingcai Liu, Hong Yang, Philippe Ciais, Yoshihide Wada
Project Administration: Wenfeng Liu
Software: Wenfeng Liu
Visualization: Wenfeng Liu
Writing – original draft: Wenfeng Liu, Xingcai Liu, Hong Yang, Philippe Ciais, Yoshihide Wada

1. Introduction

Water scarcity is the condition under which the water demands of agriculture and other economic sectors cannot be satisfied by water availability (Oki & Kanae, 2006). Cropland expansion, industrial development, and population growth have led to increasing water withdrawals and water scarcity in many regions of the world (Falkenmark, 2013; Postel et al., 1996; Qin et al., 2019; Schewe et al., 2014). Water scarcity, which is recognized as a global challenge, has been studied comprehensively since the late 1990s (J. Liu et al., 2017). The most commonly used water scarcity index (WSI) is the blue WSI (hereafter referred to as the WSI_{BW}), which is defined as the supply/availability ratio of blue water, where blue water is usable freshwater from streams, lakes, and groundwater. Current estimates of the WSI_{BW} indicate severe water scarcity in the central and southwestern parts of the United States (US), Mexico, North Africa, parts of the Middle East, North China, Northwest India, and Pakistan (Gosling & Arnell, 2016; Greve et al., 2018; Hanasaki et al., 2013a, 2013b; X. Liu, Tang, et al., 2019).

Precipitation over land differentiates into blue and green water, with green water being the water "stock" as soil moisture and can be used for evapotranspiration by plants (Falkenmark & Rockström, 2010; Schyns et al., 2019). Blue (irrigation) and green water are essential for agricultural production. Although green water alone accounts for approximately 85% of crop water use worldwide (Hoekstra & Mekonnen, 2012; J. Liu et al., 2009), it has often been overlooked in water resources and scarcity assessments (J. Liu et al., 2017). A common reason is that green water is taken for granted, while only blue water is considered to be in limited supply for human use.

Nevertheless, with increasing recognition of the importance of green water, green water scarcity assessments have been conducted (Schyns et al., 2015). Compared with blue water scarcity, the definition of green water scarcity is more complex and lacks consensus. For instance, Xu and Wu (2018) defined green water scarcity as the fraction of green water resources remaining available for non-cropland managed ecosystem services (wood production and pasture) after the demand for cropland is met. Schyns et al. (2019) defined a green WSI as the

Writing – review & editing: Wenfeng Liu, Xingcai Liu, Hong Yang, Philippe Ciais, Yoshihide Wada

ratio of green water flow allocated to plants grown with an economic value to the total green water availability; however, this ratio reflects the fraction of water being used by plants in managed lands rather than the actual water limitation of economic services. More broadly, other studies have investigated the sustainability of green water indirectly by assessing water scarcity through the introduction of alternative indicators. For example, Yano et al. (2016) used a "water unavailability" factor to indicate the impact of crop water use on source-specific water sustainability. Tuninetti et al. (2019) proposed a "water debt" indicator to measure the time required to replenish the water resources used for annual crop production. The above studies on green water sustainability have, to some extent, highlighted the importance of green water in the context of water scarcity. However, the relationship between green water use and availability and its connection with blue water has not been addressed clearly. Moreover, changes in green water availability and demand over time in agricultural production have not been considered in previous studies.

In addition to assessing blue and green water scarcity separately, there have been some attempts to combine them in an integrated water scarcity assessment. Gerten et al. (2011) and Rockström et al. (2009) compared the annual per capita shares of blue water supply and green water supply to the amount of water required to produce a standard daily diet of 3,000 kilocalories per capita to determine the water stress status of a country. This metric measures the number of people competing for a unit of water availability (blue and green) per annum (capita m^{-3} yr^{-1}), or water availability per capita (m^3 $capita^{-1}$ yr^{-1}), which is linked to a set of predefined thresholds based on basic human needs, such as a normal diet. However, a limitation of this approach is that it ignores differences in per capita water consumption across regions. In addition, a direct addition of blue and green water availabilities may not be appropriate because the presentation of blue water is in flux, while green water is in stock. To date, appropriately incorporating blue and green water in water scarcity assessment remains a key challenge (J. Liu et al., 2017). Building such an integrated index is important for gaining a more complete picture of the water scarcity status and for comparing different regions with a consistent metric. On the other hand, water scarcity is mainly due to agricultural water use, but its quantification is complicated because crop water use includes both soil moisture and irrigation. In addition, the temporal evolution of agricultural water scarcity, considering both blue and green water, is still unclear on a global scale.

To address the above research gaps, this study constructed an *agricultural green + blue water scarcity index* (hereafter referred to as the WSI_{AW}) by incorporating blue water and green water explicitly. The long-term trend of the WSI_{AW} was then examined for the period 1971–2010. Using this index, we assessed water scarcity on a global scale at the grid cell level and river basin level. Given the fact that green water is mainly used for the agricultural sector and that crop irrigation consumes the largest proportion of blue water withdrawals (Hoekstra & Mekonnen, 2012), the proposed WSI_{AW} focuses on crop production by linking the crop water demand and total water availability (both blue and green) for evapotranspiration (ET). Such a focus reflects the fact that global water scarcity is mainly related to food production (Savenije, 2000). The study was structured as follows: (a) Construction of the WSI_{AW} to provide a more complete and consistent assessment of water scarcity status across regions as opposed to blue water only or the separation of blue and green water assessments. (b) Assessment of water scarcity conditions based on the WSI_{AW}, and a comparison of the WSI_{AW} and WSI_{BW} calculated using the conventional method at the grid cell level and for 228 hydrological basins worldwide, thus providing insight into the importance of green water in determining the integrated water scarcity status. (c) Examination of the temporal evolution of the WSI_{AW} during 1971–2010 at the river basin level to determine the trends and fluctuations compared with those of the WSI_{BW}. (d) Identification of major factors driving changes in water scarcity across regions by considering green water availability for ET, crop water demand, and irrigation water use efficiency. This study is novel in that it is the first time that an integrated green + blue WSI is constructed as a consistent metric and used in global and regional assessments over time, focusing on agriculture. This approach improves the representation of global water scarcity, particularly in regions where green water dominates agricultural water supply and use. This study highlights the spatiotemporal features of the proposed WSI_{AW} that differ from previous indicators, and provides deeper insight into the severity of water scarcity on a global scale.

2. Materials and Methods

2.1. Rethinking Water Scarcity

The traditional WSI_{BW} is generally defined as the ratio of total water withdrawals for irrigation and other sectors to the total blue water availability above some minimum environmental flow requirements (J. Liu et al., 2017):

$$WSI_{BW} = \frac{IWW + BWW_{os}}{BWA - EFR}, \quad (1)$$

where WSI_{BW} [–] is the WSI based on blue water only; IWW [$km^3\ yr^{-1}$] is irrigation water withdrawal; BWW_{OS} [$km^3\ yr^{-1}$] is blue water withdrawal for other sectors, including domestic, livestock, electricity, manufacturing, and mining; BWA [$km^3\ yr^{-1}$] is the total blue water availability; and EFR [$km^3\ yr^{-1}$] is the minimum environmental flow blue water requirement. Green water is ignored in Equation 1. As green water is tightly associated with crop production, ignoring it in an assessment can lead to underestimation or overestimation of the severity of water scarcity across regions.

Blue and green water have different temporal and spatial availabilities and uses. Considering that agriculture is the only sector in which blue and green water both contribute mutually, and that this sector dominates the total water use globally, we propose a new index called the WSI_{AW} as the ratio of the crop water demand represented by crop ET under the condition of no water limitation (ETc) to the sum of green water availability for ET over cropland and blue water after the EFR and water demands of other sectors have been met:

$$WSI_{AW} = \frac{\sum_{i=1}^{n} ETc_i}{\sum_{i=1}^{n} GWA_{ET,i} + BWA_{ET}} \quad (2)$$

$$BWA_{ET} = (BWA - EFR - BWW_{os}) \times IE, \quad (3)$$

where WSI_{AW} [–] is the agricultural green + blue WSI; ETc_i [$km^3\ yr^{-1}$] is the crop ET under the condition of no water limitation for crop i; n is the number of crops considered; $GWA_{ET,i}$ [$km^3\ yr^{-1}$] is the green water availability for ET during the growing season of crop i, defined as the water supply derived from soil moisture in the rooting depth of the soil column over cropland; and BWA_{ET} [$km^3\ yr^{-1}$] is the blue water availability for ET. In this study, BWA_{ET} was scaled by the irrigation efficiency (IE) to account for water losses through percolation and evaporation during conveyance and application, and water undelivered to crops. The country-specific IE was derived from Rohwer et al. (2007). For a specific crop, variables relating to green water in Equation 2 (ETc and GWA_{ET}) were only considered during the growing season. As multi-crops were included in this study (19 crops in total), a crop water demand over the entire year could exist for a given grid cell. Therefore, variables related to blue water in Equation 2, namely BWA, EFR, and BWW_{OS}, were treated as annual fluxes. It should be noted that the ETc used in this study is not crop consumptive water use. Instead, it represents the potential crop water requirement without water limitation. The WSI_{AW} is the ratio of the crop water requirement to the total water availability for crops, while the WSI_{BW} is defined as the ratio of the sectoral water withdrawal to the total BWA. Both of these indices measure the degree to which water availability can meet water requirements, and were compared in this study.

ETc refers to a crop-specific ET corresponding to no water stress. In previous studies, actual ET (AET) was used to indicate water requirements for croplands (J. Liu et al., 2009; W. Liu et al., 2019; Quinteiro et al., 2018). AET is ET under actual water availability conditions, which could be lower than ETc due to possible water limitation. In fact, AET can be estimated by multiplying ETc by the water stress coefficient (Allen et al., 1998). However, crop water requirements should be maintained at the level of ETc even with water limitation, for example, under rainfed conditions. Therefore, using AET may lead to underestimation of agricultural water scarcity because AET is already downregulated under stressed conditions. Devineni et al. (2013) used the same method to define agricultural water demand without distinguishing rainfed and irrigated conditions, while Zhu et al. (2019) explicitly treated ETc as the agricultural water demand under rainfed conditions. We estimated ETc as the product of a crop-specific coefficient and potential ET (PET), where PET is the evaporative demand of the atmosphere, independent of crop type, crop development, and management practices (Wang & Dickinson, 2012). In addition to using PET, the reference ET (ET0) value, which was calculated based on the Food and Agriculture Organization (FAO) method (Allen et al., 1998), was also used to estimate ETc for comparison.

It should be noted that the WSI_{AW} defined here is a "crop-based" WSI, justified by the dominant role of crop production in water use in many regions. Considering the increasing attention given to water management at the river basin level, we assessed water scarcity globally using the WSI_{AW} compared with the WSI_{BW} at the grid cell level (0.5 arc degree) and river basin level. A total of 228 river basins based on the FAO GeoNetwork (http://www.fao.org/geonetwork/srv/en/metadata.show?id=38047) were considered. We aggregated the volumes of IWW, ETc,

GWA_{ET}, BWA, EFR, and BWW_{OS} for each river basin from gridded datasets (see Section 2.4) and estimated the WSI_{BW} and WSI_{AW} for each basin using Equations 1 and 2.

2.2. Identifying Crop Growing Stages

According to Allen et al. (1998), the growing season of each crop includes the initial stage, development stage, middle stage, and late stage. The crop-specific unstressed evaporation coefficients vary at different stages. In this study, we considered 19 crops that corresponded to the most important crops globally and calculated their water demands during their growing seasons. These crops include barley, cassava, citrus, cotton, grapes, groundnut, maize, millet, potato, pulses, rapeseed, rice, rye, sorghum, soybean, sugar beet, sugar cane, sunflower, and wheat. Multi-growing seasons were also considered, for instance, three seasons for rice, according to Portmann et al. (2010). Nineteen crops occupy 80% of the global total cropland (http://www.fao.org/faostat/en/#home). The growing season lengths (days between planting and harvesting dates) for the 19 crops were obtained from the MIRCA2000 dataset (Portmann et al., 2010) and subdivided into four growing stages. Accumulated fractions (Table S1 in Supporting Information S1) of the entire growing season lengths were used to determine the end dates of these four stages:

$$DOY_{s,end} = DOY_p + int(f_s \times GSL) \tag{4}$$

where $DOY_{s,end}$ [day of a year] is the last day of stage s; s can be initial (*ini*), development (*dev*), middle (*mid*), or late (*lat*) based on the growth stage; DOY_p [day of a year] is the planting date; f_s [–] (unitless) is the fraction of the length from the planting date to the last date of stage s [days] to the total growing season length (*GSL*) [days].

2.3. Definitions of Water Availability and Uses

2.3.1. Crop Water Demand

The unstressed crop water demand ETc was calculated from the product of PET using crop-specific coefficients. For a given crop, Allen et al. (1998) suggested the initial crop coefficient (K_{ini}), middle crop coefficient (K_{mid}), and end crop coefficient (K_{end}) (Table S1 in Supporting Information S1). The crop coefficients are assumed to be constant at the values of K_{ini} and K_{mid} during the initial and middle stages, whereas they vary linearly between K_{ini} and K_{mid} for the development stage and between K_{mid} and K_{end} for the late stage. The crop coefficients for each day during the development and late stages were estimated as follows:

$$K_{dev,d} = K_{ini} + \left(\frac{d - L_{ini}}{L_{dev}}\right) \times (K_{mid} - K_{ini}) \tag{5}$$

$$K_{lat,d} = K_{mid} + \left(\frac{d - (L_{ini} + L_{dev} + L_{mid})}{L_{lat}}\right) \times (K_{end} - K_{mid}), \tag{6}$$

where $K_{dev,d}$ [–] [unitless] is the crop coefficient in the development stage *dev* on day d of the growing season, and $K_{lat,d}$ [unitless] is the crop coefficient in the late stage (*lat*) on day d of the growing season; L_{ini}, L_{dev}, L_{mid}, and L_{lat} [days] are the lengths of the initial, development, middle, and late stages, respectively.

For crop i, the water demand throughout the growing season is the sum of the water demands in the four stages:

$$\mathrm{ETc}_i = 10 \times A_i \times \sum_{d=1}^{GSL} (K_{i,d} \times \mathrm{PET}_d), \tag{7}$$

where $K_{i,d}$ [unitless] is the crop coefficient of crop i on day d within the growing season; PET_d (mm d^{-1}) is the potential ET on day d; A_i [ha] is the area of crop i; and the number 10 is the unit transformation. As multiple crops were considered in this study, we summed the ETc across different crops to obtain the total water requirements of multiple crops in a grid cell.

2.3.2. Green Water Availability

We transferred green water resources from stock to flow regulated by the soil moisture content, wilting point, field capacity, and maximum daily soil water supply. Based on Gerten et al. (2007), when soil moisture is saturated,

GWA_{ET} reaches a maximum daily soil water supply (5–7 mm d^{-1}), reflecting the maximum transpiration of plants under various climatic conditions. Otherwise, GWA_{ET} is linearly scaled between the wilting point and field capacity by the actual rooting zone soil moisture content and becomes zero when the soil moisture content is lower than the wilting point:

$$GWA_{ET,i} = 10 \times A_i \times WS_{max} \times \sum_{d=1}^{GSL} R_{SM,d} \tag{8}$$

$$R_{SM,d} = \begin{cases} 1 & when\ \ SM_d \geq FC \\ \dfrac{SM_d - WP}{FC - WP} & when\ \ WP \leq SM_d < FC \\ 0 & when\ \ SM_d < WP \end{cases}, \tag{9}$$

where $GWA_{ET,i}$ [$km^3\ yr^{-1}$] is the green water availability (accounting for soil moisture up to the rooting depth) for the ET of crop i during the growing season; $R_{SM,d}$ [unitless] is the ratio of the difference between the actual rooting zone soil moisture content (SM_d) [mm] and wilting point (WP) [mm] to the difference between the field capacity (FC) [mm] and WP on day d; WS_{max} [mm d^{-1}] is the maximum daily water supply from green water. In this assessment, we used 6 mm d^{-1} for WS_{max}. After transformation, the volume of GWA_{ET} and the volume of blue water resources were of the same dimension, and thus could be summed directly.

2.3.3. Renewable Blue Water Availability, Environmental Flow Requirements, and Others

The total renewable BWA ($km^3\ y^{-1}$) was defined as the total surface and subsurface runoff. We followed the variable monthly flow (VMF) method (Pastor et al., 2014) to estimate the EFR. Here, 60% of water resources were allocated as the EFR during low flow months (monthly flow: <0.4 times the long-term average); 45% of water resources were allocated for medium flow months (monthly flow: 0.4–0.8 times the long-term average); and 30% of water resources were allocated for high flow months (monthly flow: >0.8 times the long-term average). A global application has shown that the VMF method performs well in representing locally estimated EFR values (Pastor et al., 2014). Monthly EFRs were aggregated to obtain the annual EFRs in each grid. The blue water availability for crops, BWA_{ET}, was calculated as BWA minus the sum of EFR and BWW_{OS}, multiplied by IE to account for water losses during conveyance and irrigation.

2.4. Data Sources

We conducted the analysis at a spatial resolution of 0.5 arc degree for the period from 1971 to 2010 at both monthly and annual timescales. Monthly PET and BWA were simulated by four large-scale hydrological models, namely H08 (Hanasaki et al., 2018), LPJmL (Sitch et al., 2003), PCR-GLOBWB (Wada et al., 2014), and WaterGAP2 (Müller Schmied et al., 2016), at a spatial resolution of 0.5 arc degree. The formulas for estimating PET by the four hydrological models are provided in Text S1. The four models performed historical simulations for the Inter-Sectoral Impact Model Intercomparison Project (ISIMIP, http://www.isimip.org) Phase 2a forced by the WFDEI climate data (Weedon et al., 2014). Monthly water withdrawal data for IWW and BWW_{OS} were provided by Huang et al. (2018) at a spatial resolution of 0.5 arc degree. This water withdrawal data set was reconstructed from reported data of the FAO AQUASTAT and the US Geological Survey (USGS) and simulated irrigation water withdrawal from ISIMIP 2a simulations. Annual data for domestic, electricity, mining, manufacturing, and livestock sectors from AQUASTAT and the USGS were downscaled to a monthly scale, while the irrigation water withdrawal from ISIMIP 2a simulations by the above-mentioned four hydrological models were corrected using data reported by AQUASTAT and the USGS. Huang et al. (2018) provided four different sets of irrigation water withdrawal estimates based on four hydrological models, and the mean values of the four sets were used to estimate water scarcity.

The annual variation of the cropland area during the assessment period was based on land use data set used in ISIMIP2a (Fader et al., 2010), which were derived from the HYDE 3.0 data set (Klein Goldewijk & van Drecht, 2006) and the MIRCA2000 data set (Portmann et al., 2010). The time series of the HYDE 3.0 total cropland

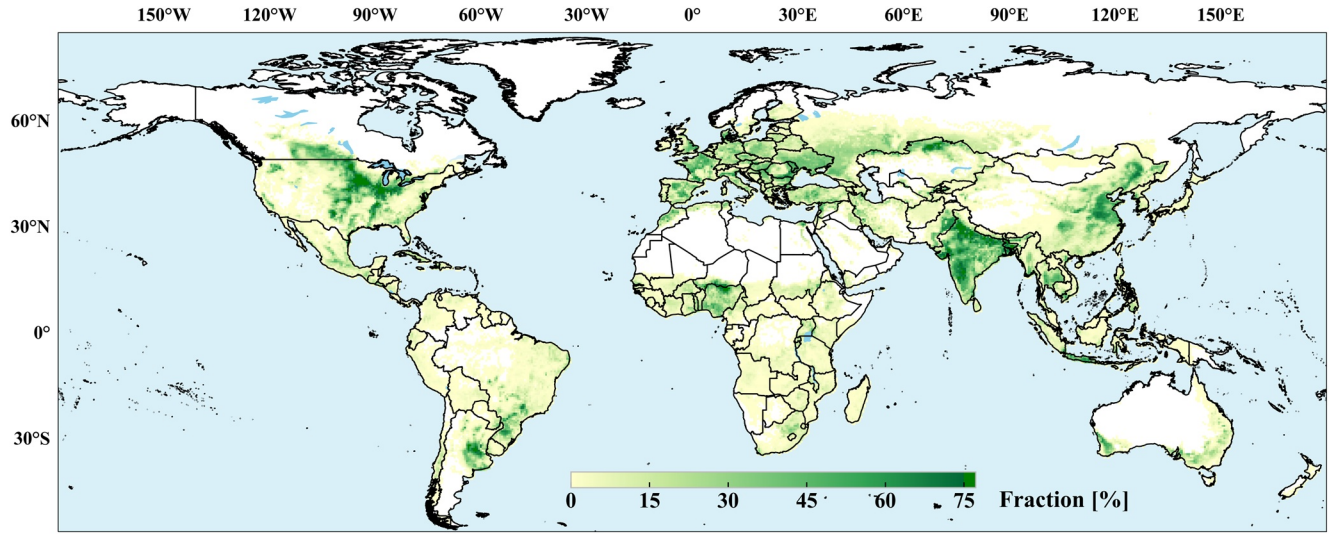

Figure 1. Fraction of cropland coverage averaged over the period 1971–2010. All 19 crops are included here.

area was allocated to each crop with the fraction from MIRCA2000 assuming that the fraction remained constant over time. Figure 1 presents the average fraction of total cropland coverage during 1971–2010, while Table 1 shows the mean irrigated, rainfed, and total cultivation areas of 19 crops over the study period. In addition to the total land coverage, this cropland data set also provides information on rainfed and irrigated cultivation areas separately (Figure S1 in Supporting Information S1). The growing seasons of the selected 19 crops across different regions were obtained from the MIRCA2000 data set, including multi-cropping systems. The field capacity and wilting point data were downloaded from the Spatial Data Access Tool (SDAT) of NASA EarthDATA (https://webmap.ornl.gov/ogcdown/dataset.jsp?ds_id=569&startPos=0&maxRecords=20&orderBy=variables&bAscend=true). The monthly rooting zone soil moisture was provided by the PCR-GLOBWB model. All the data sets mentioned above were provided at a spatial resolution of 0.5 arc degree.

Table 1
Average Values of Crop-Specific Cultivation Areas, Crop Water Demand (ETc), and Green Water Availability for Evapotranspiration (GWA_{ET}) Over the Period 1971–2010

	Irrigated area (Mha)	Rainfed area (Mha)	Total area (Mha)	ETc (km^3 yr^{-1})	GWA_{ET} (km^3 yr^{-1})
Barley	3.6	49.2	52.9	225.4	308.7
Cassava	0.0	27.1	27.1	252.3	188.5
Citrus	3.0	17.3	20.3	172.4	149.0
Cotton	13.6	45.6	59.3	536.9	327.6
Grapes	1.9	20.2	22.1	185.6	145.1
Groundnut	2.7	16.5	19.2	114.6	62.4
Maize	22.6	115.1	137.7	865.8	755.0
Millet	1.3	28.8	30.1	177.8	63.6
Potato	0.3	2.0	2.3	13.6	13.5
Pulses	4.3	55.4	59.7	335.3	164.1
Rapeseed	2.7	19.0	21.7	87.6	80.1
Rice	46.1	52.6	98.7	717.1	464.3
Rye	0.3	10.2	10.6	47.6	97.6
Sorghum	2.6	33.5	36.0	239.4	124.8
Soybean	4.6	63.8	68.4	505.1	491.9
Sugarbeet	0.9	2.7	3.6	22.7	18.9
Sugarcane	8.9	10.5	19.5	335.2	173.5
Sunflower	0.9	18.9	19.9	117.9	105.3
Wheat	43.9	141.3	185.2	1,051.1	1,219.7
Total	164.4	729.7	894.1	6,003.4	4,953.7

2.5. Trend and Uncertainty Analyses

We used the Theil-Sen slope (Sen, 1968) to estimate the trends of the WSI_{AW} and WSI_{BW}, as well as their influencing factors over the study period. The Theil-Sen method calculates the slope as the median value of all slopes between paired values and provides a robust estimation of the linear slope. A positive slope indicates an increasing trend, whereas a negative slope indicates a decreasing trend.

In addition to the trend analysis, we also conducted an uncertainty analysis of the two water scarcity indices because large-scale hydrological models are subject to high uncertainties in PET (W. Liu et al., 2016) and BWA (X. Liu, Liu et al., 2019) estimations, resulting in substantial uncertainties in the WSI assessments (Greve et al., 2018; Schewe et al., 2014). In this study, the impacts of different values of IWW, PET, and BWA derived from the four hydrological models mentioned above on water scarcity estimation were considered. We plotted the mean WSI_{BW} and WSI_{AW} values along with their standard deviations to show the corresponding uncertainties in nine major river basins across different continents. The nine major river basins were selected by choosing at least one basin on each continent, except Antarctica.

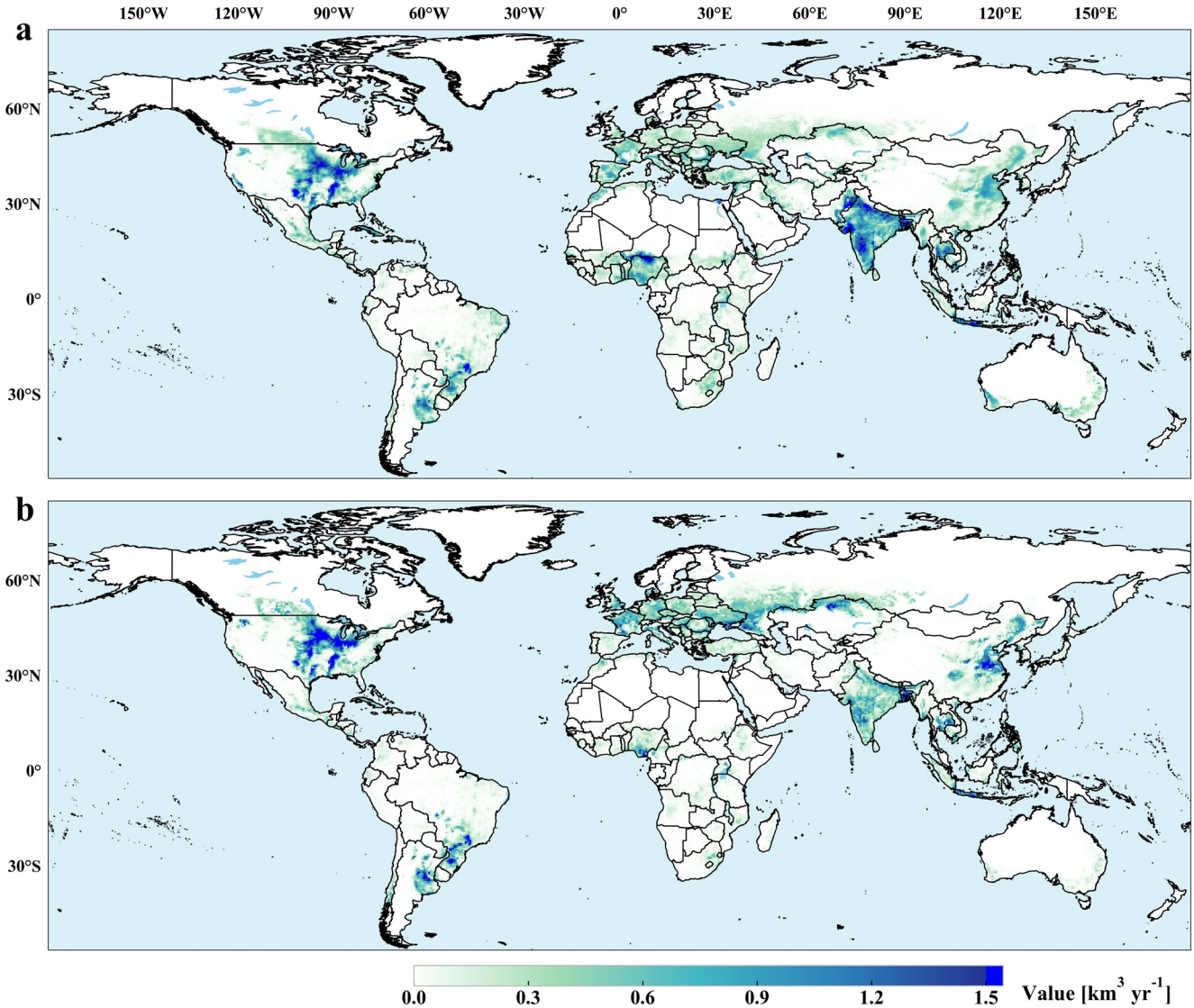

Figure 2. Crop water demand (ETc, a) and green water availability for evapotranspiration (GWA_{ET}, b) over the growing season averaged over the period 1971–2010.

3. Results

3.1. Water Demand and Availability

The average of global total ETc of the selected 19 crops over the period 1971–2010 was estimated to be 6,003 km^3 yr^{-1} (Table 1). Wheat accounted for the largest proportion (18%) of the estimated ETc, followed by maize (14%) and rice (12%). These results were consistent with their fractions in cropland coverage. The global GWA_{ET} was estimated to be 4,954 km^3 yr^{-1} for the same period. Croplands of wheat, maize, and soybean collectively contributed the largest fraction (50%) of the total GWA_{ET}.

The ETc and GWA_{ET} values showed similar spatial distributions (Figure 2) because they were both associated with cropland areas (Figure 1). The areas with high ETc and GWA_{ET} values were distributed in the middle of the US, parts of India, and southern Brazil, with values exceeding 1.5 km^3 yr^{-1} per grid for the study period due to high levels of cultivation. High values were also found in some hotspot regions in Africa, for example, in Nigeria.

The difference between GWA_{ET} and ETc represents the green water deficit to meet the optimal crop water demand. Although GWA_{ET} exceeded ETc in the eastern US, Europe, and Japan (Figure 3a), this does not mean that irrigation was not required in these regions. This is because both parameters were measured for the entire growing

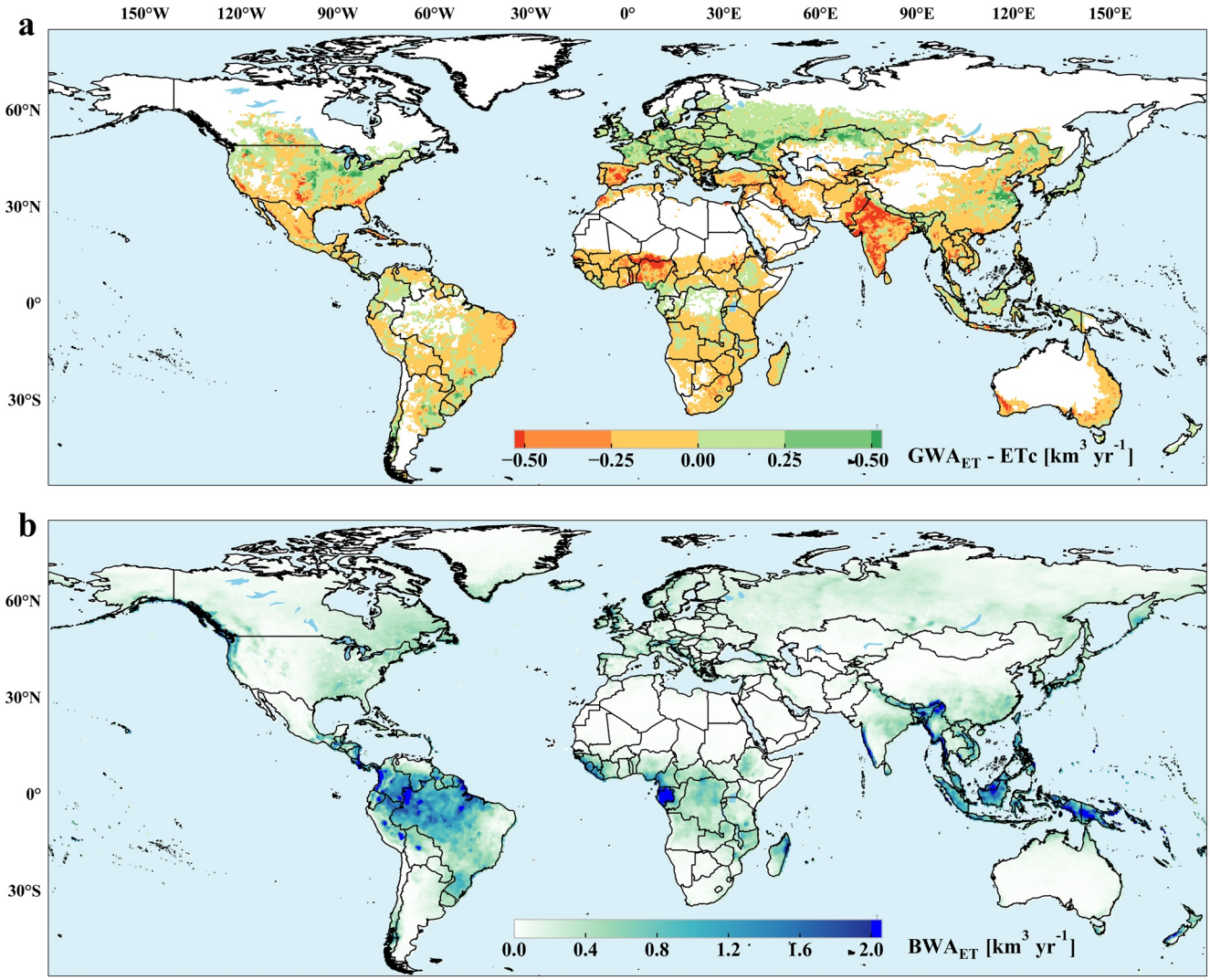

Figure 3. Difference between green water availability for crop evapotranspiration and crop water demand (GWA_{ET} - ETc, a) and blue water irrigation availability for crop evapotranspiration (BWA_{ET}, b) averaged over the period 1971–2010.

season and ETc could exceed GWA_{ET} in some specific stages, for example, the middle stage with a high crop coefficient (Table S1 in Supporting Information S1). In contrast, many regions had GWA_{ET} values below the ETc values, for example, Mexico, most of sub-Saharan Africa, the Middle East, South Asia, and Australia. This deficit of green water to meet ETc was especially high in India, which was mainly contributed by wheat, rice, and pulse cultivation (Figure S2 in Supporting Information S1). The observed GWA_{ET} in these regions was insufficient to meet the water demand of the rainfed croplands, resulting in a reduction in crop growth due to water stress in the absence of irrigation.

Figure 3b reveals an abundance of BWA_{ET} along the equator, particularly in the Amazon River basin and Southeast Asia, where BWA_{ET} reached 2.0 km^3 yr^{-1} per grid cell. In central Africa, southeast China, eastern India, and other countries in South Asia, the BWA_{ET} values were also relatively high (>0.5 km^3 yr^{-1} in each grid cell). However, regions with high BWA_{ET} values did not match the intensity of agricultural areas, as indicated by the spatial patterns of croplands in Figure 1. This was mainly because high BWA_{ET} values were observed in tropical regions, where there are no major cropland areas. For example, the regions with abundant blue water resources, such as the Amazon basin and Southeast Asia, have cropland coverages of <15%. Regions where ETc exceeded GWA_{ET} were generally those with relatively low BWA_{ET} values, thereby further exacerbating water scarcity.

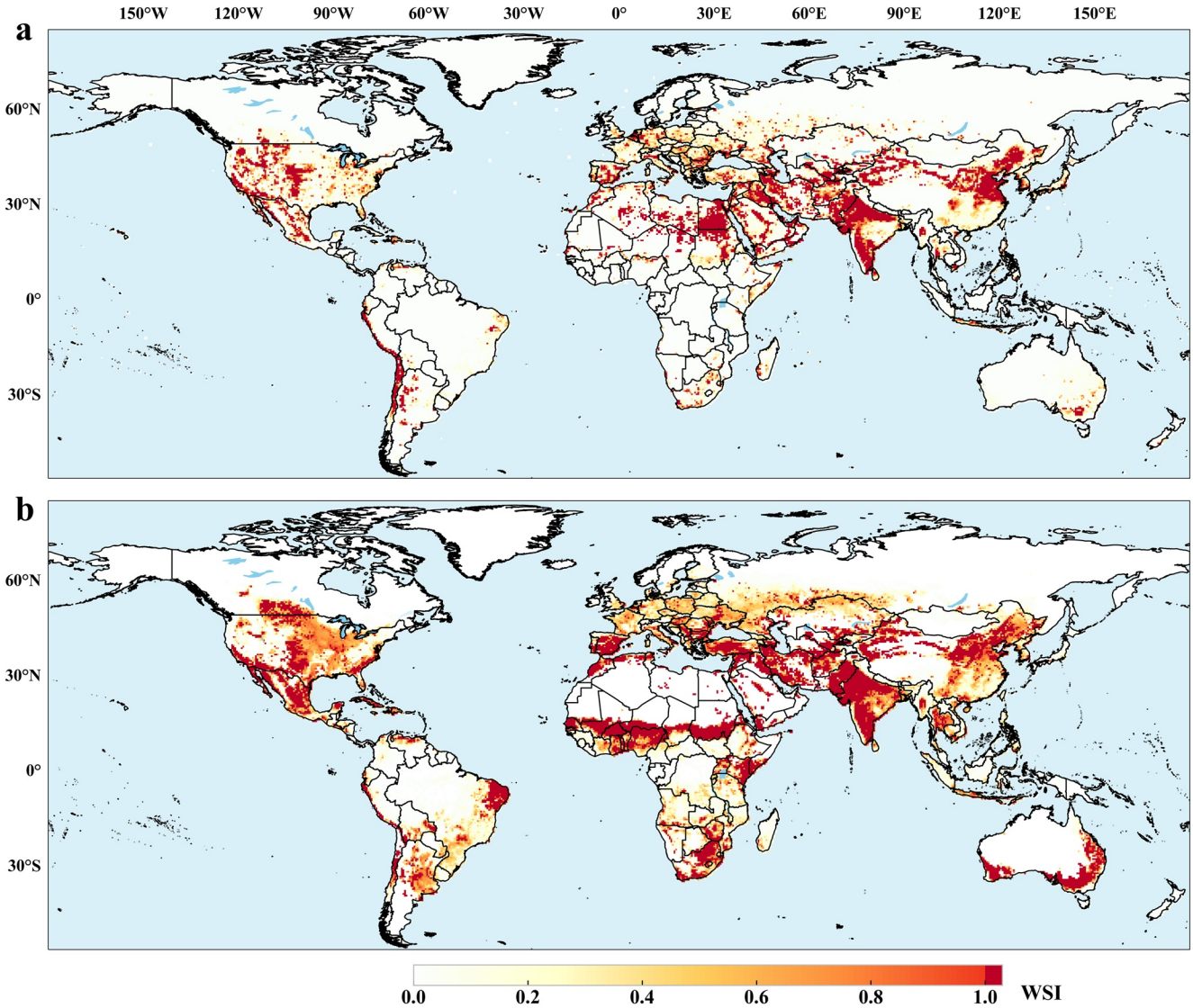

Figure 4. Comparison of the water scarcity indices based on blue water only (WSI_{BW}, a) and agricultural green + blue water (WSI_{AW}, b) at the grid cell level averaged over the period 1971–2010.

3.2. Water Scarcity Indices at the Grid Level

Overall, both the WSI_{BW} and WSI_{AW} values at the grid level indicated severe water scarcity in Pakistan, India, North China, the Middle East, and southwestern parts of the US (Figure 4). However, considerable differences were also observed in the spatial patterns of water scarcity estimated by the two WSIs. The WSI_{BW} (Figure 4a) indicated that the most water-scarce regions (e.g., $WSI_{BW} > 1$) were those with intensively irrigated areas (Figure S1a in Supporting Information S1) and/or low blue water resources (Figure S3a in Supporting Information S1). However, the WSI_{BW} could not properly reflect the agricultural water scarcity situation in rainfed crop areas due to the sole consideration of blue water. As rainfed croplands accounted for approximately 81% of the total cropland areas of the selected 19 crops (see Table 1 and Figure S1 in Supporting Information S1 for details), the areas of water-scarce regions indicated by the WSI_{BW} were underestimated. Considering the green water requirements in the calculation of the WSI_{AW}, the water-scarce crop areas ($WSI_{AW} > 1$) were larger and included Spain, Turkey, central parts of the US, southern Australia, eastern Brazil, and central and southern parts of Africa (Figure 4b).

In addition to the differences in spatial patterns, there were also differences in the levels of severity between the assessments based on the WSI_{BW} and WSI_{AW} (Figure 4). For example, in Libya and Egypt, the water scarcity

indicated by the WSI_{AW} was less severe than that indicated by the WSI_{BW}, which was mainly because low precipitation limited the cropland coverage (Figure 1) and GWA_{ET} (Figure 2b). Low cropland coverage corresponds to low ETc values, and therefore low WSI_{AW} values. On the other hand, with low BWA in the vast regions of Libya and Egypt, already relatively small water withdrawals for irrigation and other sectors resulted in high WSI_{BW} values. On the other hand, on the southern and northern edges of the sub-Saharan region and in Spain, eastern Brazil, and the central northern region of the US, the WSI_{AW} indicated a higher degree of water stress than the WSI_{BW}. These regions generally have intensive rain-fed crop production (Figure S1b in Supporting Information S1); therefore, the severity of water scarcity in these areas is probably predominantly induced by rain-fed crop production. This further indicates the lack of available green water for rainfed crops, which would have been under water stress.

In addition to water scarcity assessments at the annual level, we also estimated the mean monthly WSI_{BW} and WSI_{AW} during 1971–2010, as shown in Figures S4 and S5 of Supporting Information S1, respectively. The monthly WSI_{AW} values exceeding 1 covered larger areas than those with $WSI_{BW} > 1$, especially from June to September. The distribution of the number of months (Figure S6 in Supporting Information S1) with both WSI_{BW} and $WSI_{AW} > 1$ was similar to that of the annual water scarcity. In addition, a WSI_{AW} of >1 was associated with larger areas than the WSI_{BW} in at least 1 month of a year, but the duration of water scarcity based on the WSI_{AW} was lower in some hotspot regions, such as India, the Middle East, and the North China Plain.

3.3. Water Scarcity Indices at the River Basin Level

We estimated the WSI_{BW} and WSI_{AW} for the 228 basins during 1971–2010 (Figure 5). Similar to the grid cell assessment, the WSI_{AW} was associated with a larger area of water scarcity than the WSI_{BW}. Based on the WSI_{AW} and WSI_{BW}, approximately 22% and 8% of these river basins experienced water scarcity (WSI > 1), respectively. These basins covered approximately 15% and 5% of the terrestrial land areas, respectively. The WSI_{BW} and WSI_{AW} values also exhibited different spatial patterns. Basins with high WSI_{BW} values were mainly concentrated in areas around 30°N (Figure 5a) with low blue water resources (Figure S3a in Supporting Information S1) and high water withdrawals for irrigation and other sectors (Figures S7 and S8 in Supporting Information S1). In contrast, basins with high WSI_{AW} values were distributed more evenly around the globe, especially between 30°S and 45°N (Figure 5b) because this index includes the crop water demand (Figure S9a in Supporting Information S1) and total (blue and green) water availability for crop ET (Figure S10a in Supporting Information S1).

Many basins exhibited very different WSI_{BW} and WSI_{AW} values (Figure 5). The WSI_{BW} was generally low in sub-Saharan Africa and southern Australian basins, while the WSI_{AW} was relatively high in many basins of these regions. For example, the WSI_{BW} value was very low (0.03) in the Niger River basin, whereas the WSI_{AW} was 1.1. This situation often occurs in basins dominated by rainfed croplands. Therefore, the water stress in such regions with high WSI_{AW} values is responsible for the gaps between the actual crop yield and potential yield on rainfed land. In contrast, some basins dominated by irrigation cropland, such as the Haihe River basin in China, the WSI_{AW} values were lower than the WSI_{BW} values. At the monthly timescale, there were also significant differences between the WSI_{BW} and WSI_{AW} across river basins (Figure S11 in Supporting Information S1). For instance, the WSI_{AW} was higher than the WSI_{BW} in the Niger basin for the entire year. In the Danube River basin, the WSI_{AW} was higher than the WSI_{BW} in summer, whereas it was lower in winter.

3.4. Trends and Uncertainties of the Water Scarcity Indices at the River Basin Level

Over the study period, most river basins showed increasing trends in water scarcity based on both the WSI_{BW} and WSI_{AW}; however, the extent of these trends varied among the basins (Figure 6). Large increases in the WSI_{BW} (Figure 6a) were observed in basins with low blue water resources (Figure S3a in Supporting Information S1), especially in the Middle East, South Asia, and North China Plain. These increases were mainly driven by decreases in BWA (Figure S3 in Supporting Information S1) and increases in IWW (Figure S7 in Supporting Information S1) and BWW_{OS} (Figure S8 in Supporting Information S1). Increasing trends in the WSI_{AW} were also significant in these regions (Figure 6b), but of a lower magnitude compared with the trends in the WSI_{BW}. On the other hand, compared with the WSI_{BW}, a larger increase in the magnitude of the WSI_{AW} was observed in sub-Saharan Africa, Europe, and Australia. A decreasing trend (although not significant) in the WSI_{BW} in Europe was observed due to decreases in IWW and BWW_{OS}, while the WSI_{AW} exhibited a significant increasing trend because

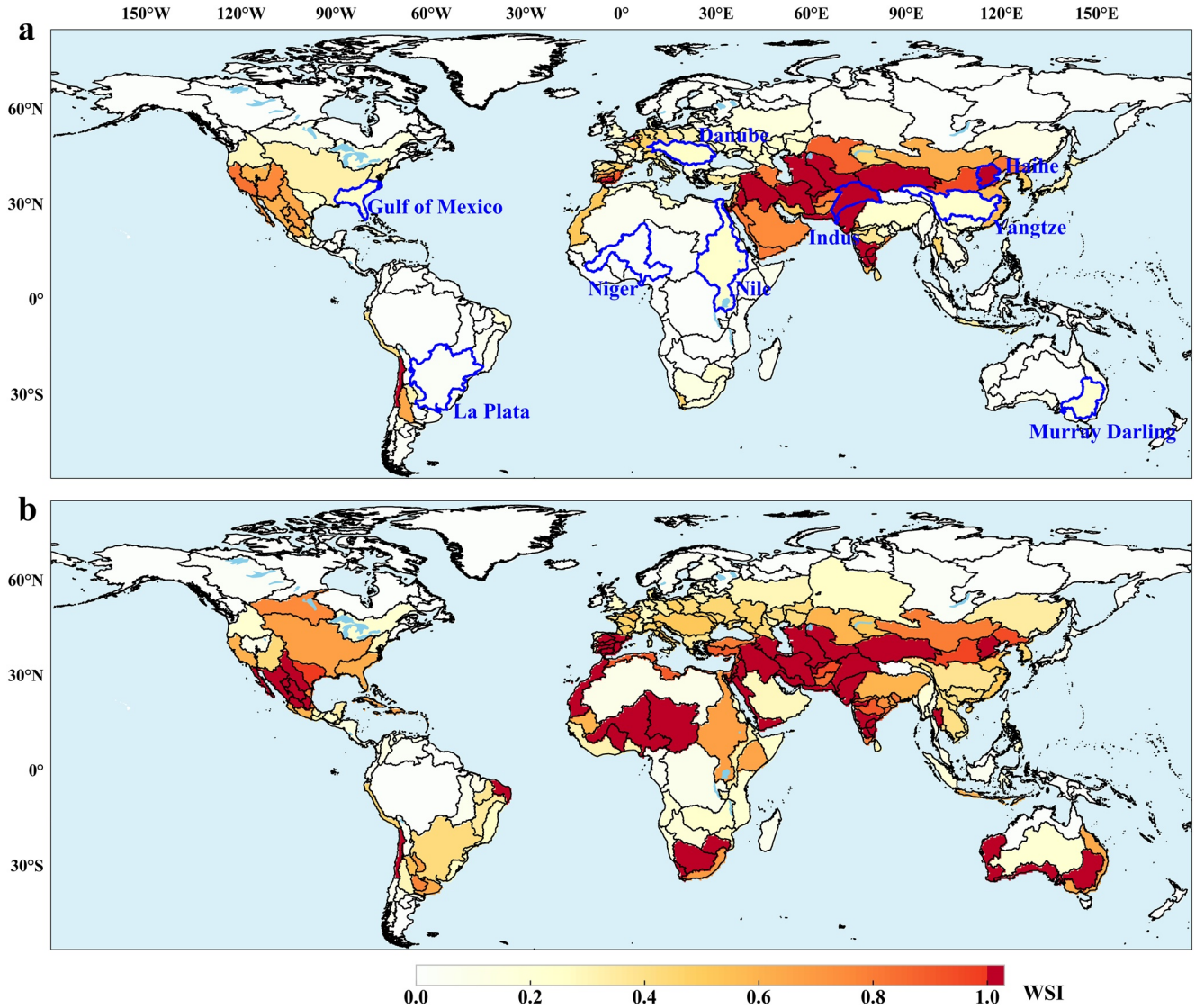

Figure 5. Comparison of the water scarcity indices based on blue water only (WSI_{BW}, a) and agricultural green + blue water (WSI_{AW}, b) at the river basin level averaged over the period 1971–2010. The locations of nine river basins used for the uncertainty analysis are outlined in blue in subplot (a).

of the climate-induced rising trend of ETc (Figure S5 in Supporting Information S1). In contrast, most basins over 45°N presented decreasing trends in both the WSI_{AW} and WSI_{BW} due to increased water resources (Figures S3 and S12 in Supporting Information S1) and decreased water use (Figures S7–S9 in Supporting Information S1).

Several different patterns of changes in the WSI_{BW} and WSI_{AW} were clearly observed for the nine selected major river basins (Figure 7). The trends for the WSI_{BW} and WSI_{AW} values were similar for the Yangtze, Nile, and Indus basins during the study period. The WSI_{AW} presented an increasing trend for the Danube basin, while the WSI_{BW} exhibited an increasing trend for the period 1971–1990 before decreasing thereafter. The Haihe basin presented a stable WSI_{AW}, whereas the WSI_{BW} exhibited an increasing trend. The trend analysis also revealed another advantage of using the WSI_{AW} instead of the WSI_{BW}, that is, the impact of changes in rainfed cropland. For example, the WSI_{AW} in the Niger basin increased considerably during the study period, while the increase in the WSI_{BW} was minor. The two water scarcity indices showed quite distinct trends in the Niger and Haihe basins, reflecting the different key factors contributing to water scarcity. The Haihe basin was mainly dominated by increasing water use for "other sectors," whereas the Niger basin was dominated by expanding cropland. This difference further highlights the relevance of using the WSI_{AW} to indicate emerging water scarcity due to cropland expansion, especially in areas of rainfed land.

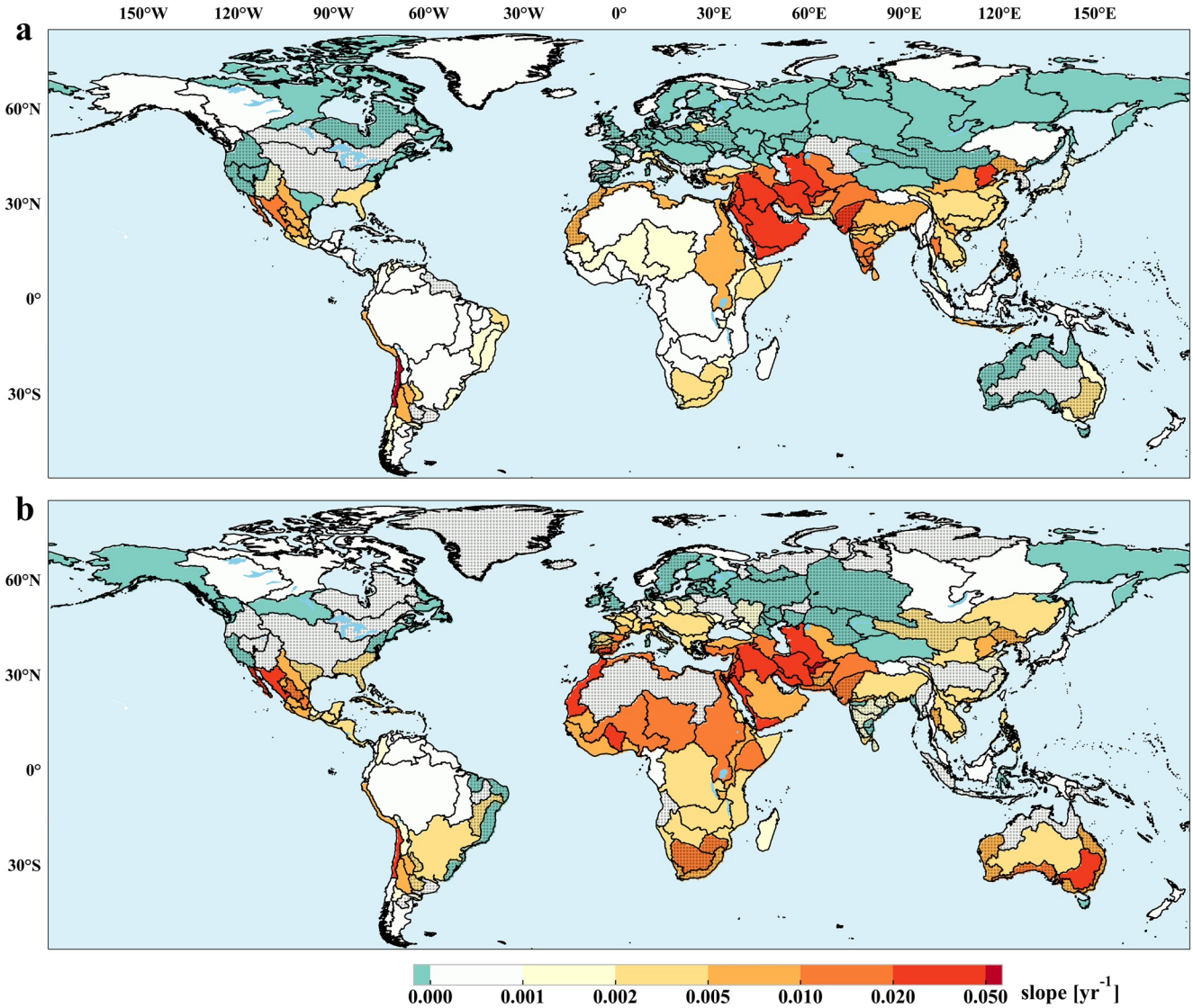

Figure 6. Trend slopes of the water scarcity indices based on blue water only (WSI_{BW}, a) and on agricultural green + blue water (WSI_{AW}, b) at the river basin level during 1971–2010. Basins with insignificant slopes (i.e., the slope is not significantly different from 0 at a significance level of 0.05) are hatched with points.

We note high uncertainties in the WSI assessments, such as high standard deviation ranges for the WSI_{AW} in the Danube basin and the WSI_{BW} in the Haihe basin (Figure 7). The coefficients of variation for the WSI_{BW} and WSI_{AW} were generally >0.3 (Figure S13 in Supporting Information S1). The uncertainties were particularly large in water-limited regions, for example, North Africa, the Middle East, and central Australia. In addition, the selection of the WS_{max} value could have affected the estimation of the WSI_{AW}. The WS_{max} value generally varies between 5 and 7 mm d^{-1}, and we set it to 6 mm d^{-1}. However, we found that the WSI_{AW} presented quite similar patterns and values when setting WS_{max} to 5 and 7 mm d^{-1} (Figure S14 in Supporting Information S1); thus, the selection of WS_{max} values in this range had little impact on the WSI_{AW} estimates.

4. Discussion

4.1. Comparison of the WSI_{AW} and WSI_{BW}

Taking agriculture as the nexus of blue and green water use, we introduced the WSI_{AW} by including both types of water resources for crop production. Given that crop production is the largest sector of water use and the main driver of water scarcity in the world, it is important to have good insight into the water scarcity status with crop

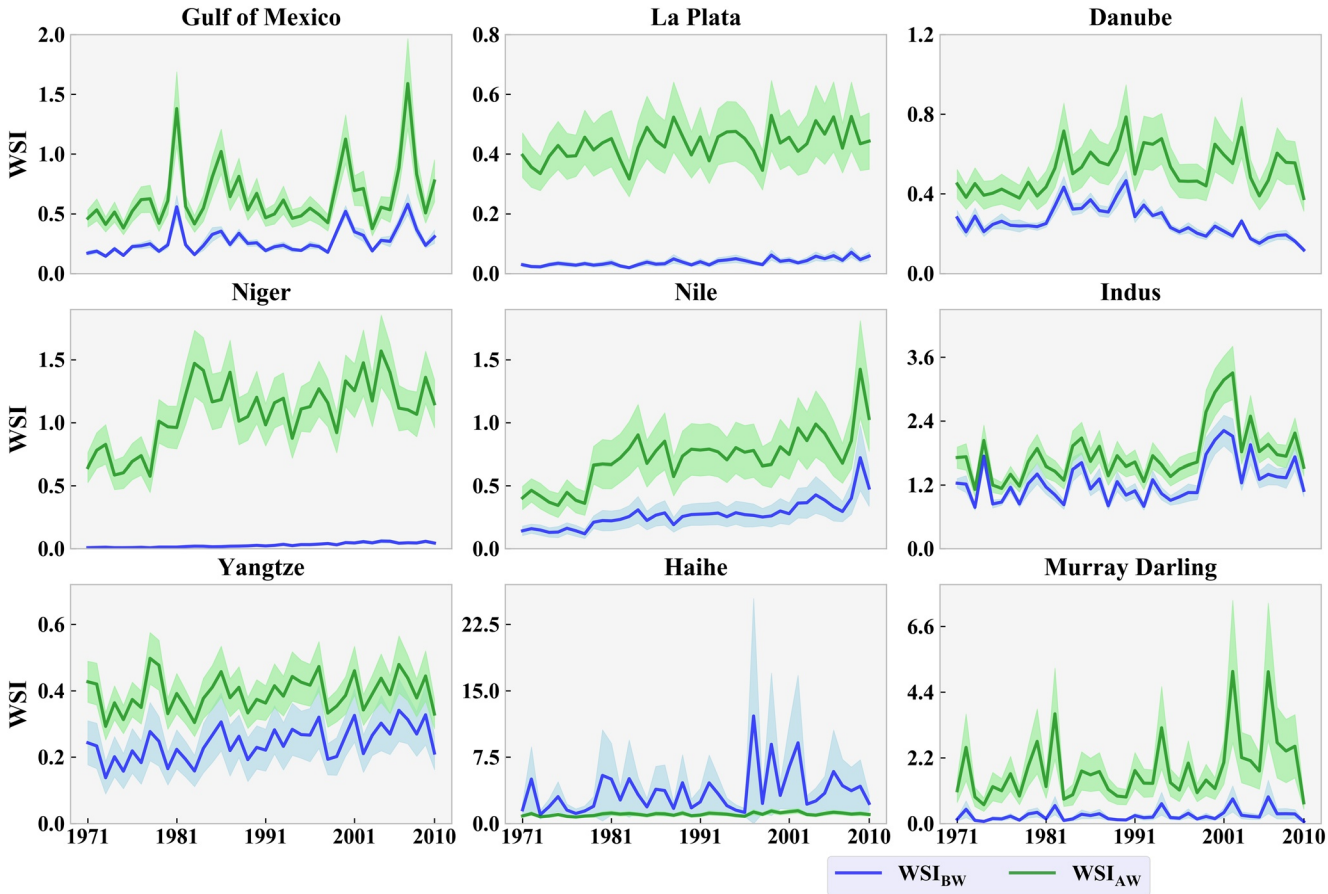

Figure 7. Evolution of the water scarcity indices based on blue water only (WSI_{BW}) and agricultural green + blue water (WSI_{AW}), and the associated uncertainties for nine river basins worldwide. The blue and green lines show the mean WSI_{BW} and WSI_{AW} values, while light blue and light green represent their ±1 standard deviation ranges. The locations of the nine river basins are shown in Figure 5a.

production water availability and use at the center of the metric. By including green water, the WSI_{AW} better reflects water scarcity in cropland areas subject to a dry climate in the growing season, which cannot be captured by the WSI_{BW}.

We found that the WSI_{AW} values were higher than the WSI_{BW} values in approximately 79% of the studied river basins, especially in those with limited irrigation withdrawal, as indicated by the low IWW/BWA ratios in Figure 8. In rainfed-dominated areas, particularly in Africa, central southern parts of the US, and the southeastern part of South America, ETc was very high, whereas GWA_{ET} was insufficient to meet the high water demand of crops (Figure 3a). Therefore, even if these regions have relatively high precipitation and/or blue water resources, they can still be water scarce based on the WSI_{AW}. This situation is typical in many parts of sub-Saharan Africa, where blue water resources are plentiful but irrigation areas are not developed; hence, the WSI_{BW} did not generally indicate water scarcity in this region. Instead, there are vast areas of parched croplands in the region, which were clearly reflected by the WSI_{AW}. Overall, 19 basins presented blue water scarcity (i.e., $WSI_{BW} > 1$); among these, 18 basins also had agricultural water scarcity (i.e., $WSI_{AW} > 1$). However, of the 47 basins with a WSI_{AW} of >1, only 18 had a WSI_{BW} of >1.

The WSI_{BW} generally increased with an increase in the IWW/BWA ratio, indicating the dominant role of irrigation water withdrawal on blue water scarcity (Figure 8). The Sabarmati River basin in India and Pakistan had the largest IWW/BWA ratio, which resulted in the highest WSI_{BW}. In contrast, the WSI_{AW} was not primarily controlled by the IWW/BWA ratio but was related to the fraction of GWA_{ET} to ETc. Generally, the lower the fraction of GWA_{ET} to ETc, the higher the WSI_{AW}. For example, the Guadiana basin had a very low fraction of GWA_{ET} to ETc (9%), and its WSI_{AW} was the highest (5.1). There are exceptions, for example, the Arabian Peninsula River basin in the

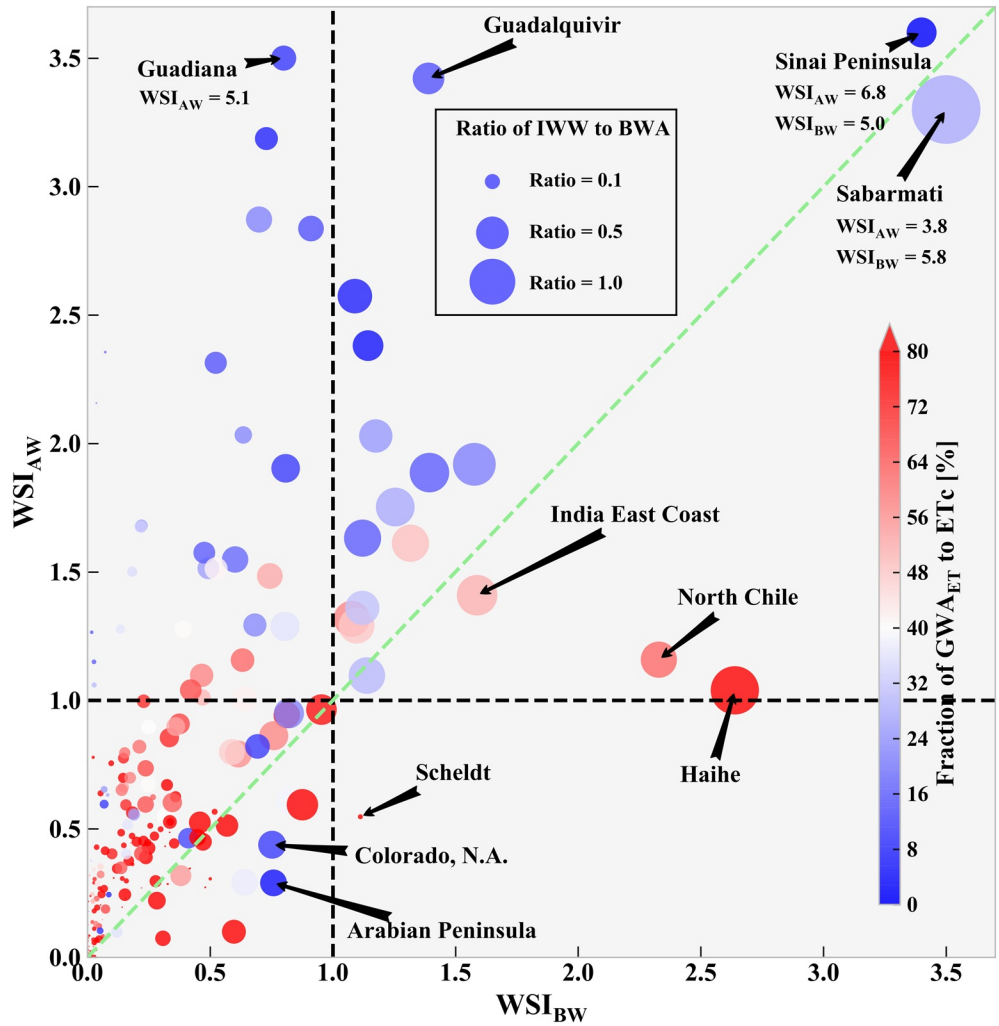

Figure 8. Comparison of water scarcity indices based on blue water only (WSI_{BW}) and agricultural green + blue water (WSI_{AW}) at the river basin level. The point size indicates the ratio of irrigation water withdrawal (IWW) to blue water availability (BWA). The color represents the fraction [%] of green water availability for evapotranspiration (GWA_{ET}) to crop water demand (ETc). For a better illustration, the WSI_{AW} and WSI_{BW} values for the Sabarmati and Sinai Peninsula basins and the WSI_{AW} value for the Guadiana basin are changed in the figure. Their true values are indicated below the basin names.

Middle East had a WSI_{AW} of 0.3, even though the GWA_{ET} could only meet 3% of its ETc. The low WSI_{AW} value in the Arabian Peninsula basin was mainly due to the small cropland area (Figure 1), meaning that ETc was much smaller than BWA (only 9%). In contrast, the Haihe basin in China had a high fraction of GWA_{ET} to ETc (89%), and its WSI_{AW} reached 1.0 because it is located in a populous and industrialized region, where 37% of BWA goes to BWW_{OS} instead of irrigation water. This ratio is extremely high compared with the global average of 3% (Rost et al., 2008). After deducting the EFR, minimal BWA_{ET} would remain for crops in the Haihe basin.

Withdrawn water for irrigation includes a fraction delivered for crop growth and losses due to leaching and evaporation during the conveyance and application processes (Jägermeyr et al., 2015). Leaching losses can be reinfiltrated to groundwater; however, it was unclear how they could be reused in the same grid, although some of them could be reused at the basin level, expressed as recoverable return flow. Therefore, the use of the IE information from Rohwer et al. (2007), which considered both leaching and evaporation losses, could have overestimated the WSI_{AW} at the river basin level in this study. This mainly relates to the lack of IE data assessing solely evaporation losses on a global scale. Moreover, we used fixed IE values for 2,000 to represent the 1971–2010 period due to unavailable long-term IE series on a global scale, and noticed that the IE values varied between 0.3 and 0.8 across river basins (Table S2 in Supporting Information S1). To illustrate the possible impact of changes

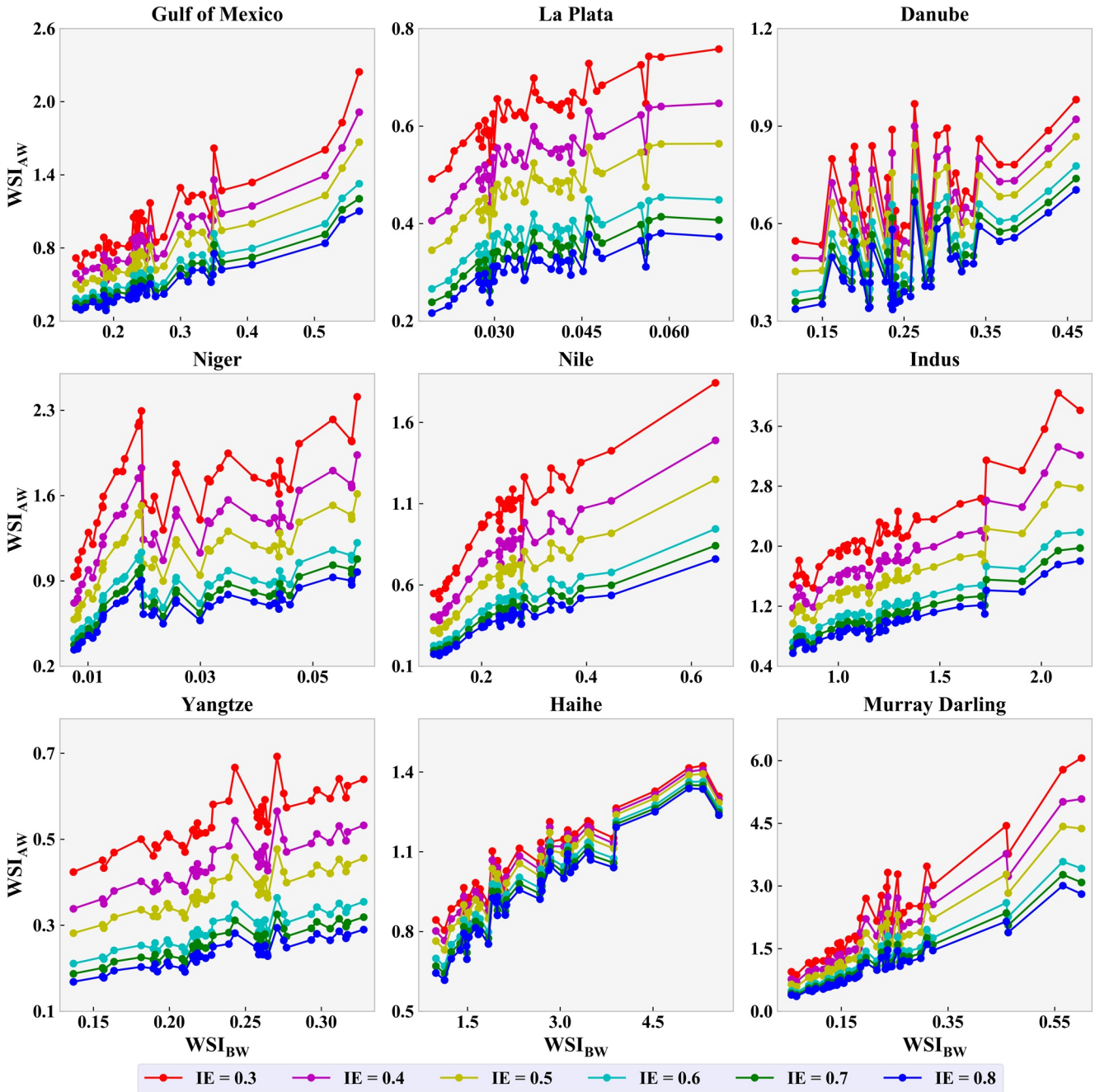

Figure 9. Impacts of irrigation efficiency (IE) on the calculation of the water scarcity index based on agricultural green + blue (WSI_{AW}), and a comparison with the water scarcity index based on blue water only (WSI_{BW}) for nine river basins worldwide. Six values of IE between 0.3 and 0.8 are selected for illustration purposes. The locations of the nine river basins are shown in Figure 5a.

in IE values on the WSI_{AW}, we recalculated the WSI_{AW} with IE ranging from 0.3 to 0.8 and plotted the WSI_{AW} against the WSI_{BW} for the nine major river basins. The results showed that different IEs could lead to changes in the WSI_{AW} (Figure 9). Although the WSI_{AW} increased with an increase in the WSI_{BW}, improving IE could reduce the WSI_{AW}, particularly in years with high water scarcity. However, improving IE would not help to decrease the WSI_{AW} in regions where other sectors already limit the amount of useable water for irrigation, such as the Haihe River basin (Figure 9).

4.2. Comparison of the WSI_{AW} With Existing Water Scarcity Indicators and the Implications

J. Liu et al. (2017) reviewed nine types of water scarcity indicators used in the literature. Only two of them considered green water: the "green-blue water scarcity" proposed by Rockström et al. (2009) and amended by Gerten et al. (2011), and the "water footprint-based assessment" of Hoekstra and Mekonnen (2012). Although green water was included in the water footprint, only blue water was used to estimate water scarcity (Mekonnen & Hoekstra, 2016). Our WSI_{AW} assessment determined severe water scarcity in the central part of the US, many regions of Africa, eastern Brazil, and southern Australia. However, none of the blue water-based WSIs indicated water scarcity in these regions. High water scarcity in Africa was only diagnosed by the "physical and economic water scarcity" and "water poverty" indices (J. Liu et al., 2017). However, water scarcity in Africa denoted by these two indicators is more due to economic constraints rather than physical water limitations. The only WSI incorporating blue and green water also failed to reflect water scarcity in vast rainfed regions, for example, in the central part of the US and in southern Australia. This was because it aims to meet the per capita water demand based on a normal diet rather than the actual crop water demand (Kummu et al., 2014).

Compared with the conventional calculation of green water availability for cropland, which is estimated from the total soil moisture content (Xu & Wu, 2018) or actual crop ET (Gerten et al., 2011), the method proposed in this study calculates GWA_{ET} based on the maximum daily water supply and a ratio incorporating the actual soil moisture content, wilting point, and field capacity. This approach converts green water from "stock" to "flow". By using ETc as the crop water demand, our proposed scarcity index can detect emerging agricultural water scarcity worldwide. As the WSI_{AW} is mainly used for agricultural water scarcity assessments, its disadvantage lies in the fact that it cannot reflect water scarcity due to water use from other sectors. The WSI_{AW} measures the extent to which blue and green water resources meet the crop water requirements. In contrast, the WSI_{BW} indicates the extent to which blue water resources can meet the blue water demand of different sectors, including agricultural irrigation. Therefore, the WSI_{AW} and WSI_{BW} were measured in different dimensions. While we emphasize the advantages of the WSI_{AW} in reflecting the status of water scarcity given that crop production is the largest water user with respect to both green and blue water, we are aware that it does not explicitly reflect the water scarcity caused by the water demand of other sectors. To this end, assessments using both indicators may provide more complete information to support water resource management.

4.3. Evolution in Water Scarcity and the Contributing Factors

Distinct spatial patterns were observed in the evolution of the WSI_{BW} and WSI_{AW} (Figure 6). Considerable increases in the WSI_{BW} were mainly observed in the Middle East, India, and eastern China. As the total blue water is relatively stable in these regions, as expressed as an insignificant trend in BWA (Figure S3 in Supporting Information S1), the increasing trend in the WSI_{BW} can be attributed to the increasing trends in water withdrawals for irrigation (Figure S7 in Supporting Information S1) and other sectors (Figure S8 in Supporting Information S1). On the other hand, the decreasing trend in the WSI_{BW} in the regions north of 30°N corresponds to the increasing BWA and decreasing IWW and BWW_{OS}. However, contributors to the evolution of the WSI_{AW} are more complex than those of the WSI_{BW} as more factors are involved, including changes in BWA, withdrawals, green water availability over croplands (both irrigated and rainfed), and crop water demand. Increasing blue water withdrawals in non-cropland production sectors (Figure S8 in Supporting Information S1) decreases the remaining BWA for crops when the total BWA is stable. This is particularly true for the regions south of 30°N, where the WSI_{AW} presented a significant increasing trend. However, GWA_{ET} and ETc contributed differently to changes in the WSI_{AW} values in these regions. For example, the increasing trends of the WSI_{AW} in the Middle East and Australia were further intensified by rising ETc and declining GWA_{ET}, while an additional contribution to the increasing WSI_{AW} in Africa was because the rate of the rising trend in ETc exceeded that of the rising trend in GWA_{ET}. Similar to the WSI_{BW}, the WSI_{AW} also exhibited a declining trend north of 30°N, which was further triggered by increasing GWA_{ET}, in addition to an increase in BWA and a decrease in BWW_{OS}.

4.4. Limitations of the Research and Outlook

In this study, we proposed the WSI_{AW} by incorporating blue and green water into the metric. The approaches for quantifying green water availability and cropland water demand presented here are applicable for assessments at

varying spatial scales. Nevertheless, we acknowledge the limitations of this approach. Most of these are related to uncertainties in the input data and estimation.

Crop ET (i.e., ETc) was used to indicate the crop water demand, implying that no stress was considered. However, this may overestimate the water demand when crop growth is constrained by other factors, such as nutrient stress, pests, or poor soil quality. This could be particularly true in Africa, where crop growth is generally limited by nitrogen inputs (W. Liu et al., 2018). Allen et al. (1998) estimated ETc based on ET0 rather than PET. We found that the ETc based on ET0 presented a spatial pattern similar to that of the ETc based on PET (Figure 2a and Figure S15 in Supporting Information S1). As a result, the global distribution of the WSI_{AW} based on PET was only slightly different from that based on ET0, mainly in the central part of the US and Argentina (Figure 4b and Figure S16 in Supporting Information S1). To illustrate the uncertainty from hydrological models, we used PET in this study. The EFR, which affects the spatial and temporal patterns of blue water resource availability, was estimated using only the VFM method. However, various EFR methods can lead to quite different estimations of EFR (Pastor et al., 2014). Hence, using different EFR estimations can significantly affect the degree of estimated water scarcity. For future studies, analyzing the basin-specific EFR by various methods would be helpful for reducing uncertainties in EFR estimations, and thus, water scarcity assessments. However, determining EFR uncertainties is complicated because the EFR exhibits temporal and spatial variations in the proportion of the mean annual flow to maintain different levels of ecological conditions (Jägermeyr et al., 2017). This would require an integrated metric or framework that simultaneously considers the interaction between conservation status and water management goals. Such detailed research is beyond the scope of this study, but should be a task for future research.

5. Conclusions

We proposed a new WSI incorporating green and blue water to assess agricultural water scarcity on a global scale for the period 1971–2010. The new index measures the degree to which the total blue and green water availability can meet the water demand for cropland. Instead of AET, ETc was used to indicate the water demand of crops. The maximum water supply from green water and a ratio integrating the actual soil moisture content, wilting point, and field capacity were used to estimate GWA_{ET}, which transfers green water availability from "stock" to "flow" to be consistent with the flux mode of blue water.

The assessment using the WSI_{AW} showed that the coverage of water-scarce areas was much broader than that of the traditional assessment focusing only on blue water, that is, 22% of river basins were found to be water scarce based on the WSI_{AW} versus 8% based on the WSI_{BW}. The comparison also revealed that water scarcity based on the proposed approach had higher values over the rainfed croplands. The main reason for this is that rainfed land also has a high water demand, but soil water is insufficient to support the demand. The expansion of croplands and the increase in water withdrawals by other sectors were the main reasons for the intensification of water scarcity during the study period, which was clear in many river basins worldwide, particularly in some Asian and African river basins. Improving IE could reduce the WSI_{AW}, especially in regions with high amounts of blue water remaining for cropland.

Conflict of Interest

The authors declare no conflicts of interest relevant to this study.

Data Availability Statement

Accesses to all data sets are as follows: the ISIMIP data (https://esg.pik-potsdam.de/projects/isi-mip/), the NASA soil data (https://webmap.ornl.gov/ogcdown), and water withdrawal data (https://zenodo.org/record/1209296#.XmEIdahKg-U).

Acknowledgments
This study was supported by the National Natural Science Foundation of China (52109071), Chinese Universities Scientific Fund (2021RC016), and the Top Agricultural Universities Partnership Collaboration Awards 2021. X.L. and H.Y. were supported by the Swiss National Science Foundation (200021_188686). P.C. was supported by the French State Aid managed by the ANR under the "Investissements d'avenir" programme with the reference ANR-16-CONV-0003. The authors are grateful to the Inter-Sectoral Impact Model Intercomparison Project (ISIMIP) for providing the global hydrological simulation data.

References

Allen, R. G., Pereira, L. S., Raes, D., & Smith, M. (1998). *Crop evapotranspiration-Guidelines for computing crop water requirements-FAO Irrigation and drainage paper 56* (Vol. 300). FAO.

Devineni, N., Perveen, S., & Lall, U. (2013). Assessing chronic and climate-induced water risk through spatially distributed cumulative deficit measures: A new picture of water sustainability in India. *Water Resources Research*, *49*(4), 2135–2145.

Fader, M., Rost, S., Müller, C., Bondeau, A., & Gerten, D. (2010). Virtual water content of temperate cereals and maize: Present and potential future patterns. *Journal of Hydrology*, *384*(3), 218–231.

Falkenmark, M. (2013). Growing water scarcity in agriculture: Future challenge to global water security. *Philosophical Transactions of the Royal Society A: Mathematical, Physical and Engineering Sciences*, *371*(2002), 20120410.

Falkenmark, M., & Rockström, J. (2010). Building water resilience in the face of global change: From a blue-only to a green-blue water approach to land-water management. *Jorunal of Water Resources Planning and Management*, *136*(6), 606–610.

Gerten, D., Heinke, J., Hoff, H., Biemans, H., Fader, M., & Waha, K. (2011). Global water availability and requirements for future food production. *Journal of Hydrometeorology*, *12*(5), 885–899.

Gerten, D., Schaphoff, S., & Lucht, W. (2007). Potential future changes in water limitations of the terrestrial biosphere. *Climatic Change*, *80*(3–4), 277–299.

Gosling, S. N., & Arnell, N. W. (2016). A global assessment of the impact of climate change on water scarcity. *Climatic Change*, *134*(3), 371–385.

Greve, P., Kahil, T., Mochizuki, J., Schinko, T., Satoh, Y., Burek, P., et al. (2018). Global assessment of water challenges under uncertainty in water scarcity projections. *Nature Sustainability*, *1*(9), 486–494.

Hanasaki, N., Fujimori, S., Yamamoto, T., Yoshikawa, S., Masaki, Y., Hijioka, Y., et al. (2013a). A global water scarcity assessment under Shared Socio-economic Pathways – Part 1: Water use. *Hydrology and Earth System Sciences*, *17*(7), 2375–2391.

Hanasaki, N., Fujimori, S., Yamamoto, T., Yoshikawa, S., Masaki, Y., Hijioka, Y., et al. (2013b). A global water scarcity assessment under Shared Socio-economic Pathways – Part 2: Water availability and scarcity. *Hydrology and Earth System Sciences*, *17*(7), 2393–2413.

Hanasaki, N., Yoshikawa, S., Pokhrel, Y., & Kanae, S. (2018). A global hydrological simulation to specify the sources of water used by humans. *Hydrology and Earth System Sciences*, *22*(1), 789–817.

Hoekstra, A. Y., & Mekonnen, M. M. (2012). The water footprint of humanity. *Proceedings of the National Academy of Sciences of the United States of America*, *109*(9), 3232–3237.

Huang, Z., Hejazi, M., Li, X., Tang, Q., Vernon, C., Leng, G., et al. (2018). Reconstruction of global gridded monthly sectoral water withdrawals for 1971–2010 and analysis of their spatiotemporal patterns. *Hydrology and Earth System Sciences*, *22*(4), 2117–2133.

Jägermeyr, J., Gerten, D., Heinke, J., Schaphoff, S., Kummu, M., & Lucht, W. (2015). Water savings potentials of irrigation systems: Global simulation of processes and linkages. *Hydrology and Earth System Sciences*, *19*(7), 3073–3091.

Jägermeyr, J., Pastor, A., Biemans, H., & Gerten, D. (2017). Reconciling irrigated food production with environmental flows for Sustainable Development Goals implementation. *Nature Communications*, *8*, 15900.

Klein Goldewijk, K., & van Drecht, G. (2006). HYDE 3. Current and historical population and land cover. In A. F. Bouwman, T. Kram, & K. Klein Goldewijk (Eds.), *Integrated modelling of global environmental change. An overview of IMAGE 2.4*. Netherlands Environmental Assessment Agency (MNP).

Kummu, M., Gerten, D., Heinke, J., Konzmann, M., & Varis, O. (2014). Climate-driven interannual variability of water scarcity in food production potential: A global analysis. *Hydrology and Earth System Sciences*, *18*(2), 447–461.

Liu, J., Yang, H., Gosling, S. N., Kummu, M., Flörke, M., Pfister, S., et al. (2017). Water scarcity assessments in the past, present, and future. *Earth's Future*, *5*(6), 545–559.

Liu, J., Zehnder, A. J. B., & Yang, H. (2009). Global consumptive water use for crop production: The importance of green water and virtual water. *Water Resources Research*, *45*(5), W05428.

Liu, W., Antonelli, M., Kummu, M., Zhao, X., Wu, P., Liu, J., et al. (2019). Savings and losses of global water resources in food-related virtual water trade. *Wiley Interdisciplinary Reviews: Water*, *6*(1), e1320.

Liu, W., Yang, H., Folberth, C., Muller, C., Ciais, P., Abbaspour, K. C., & Schulin, R. (2018). Achieving high crop yields with low nitrogen emissions in global agricultural input intensification. *Environmental Science & Technology*, *52*, 13782–13791.

Liu, W., Yang, H., Folberth, C., Wang, X., Luo, Q., & Schulin, R. (2016). Global investigation of impacts of PET methods on simulating crop-water relations for maize. *Agricultural and Forest Meteorology*, *221*, 164–175.

Liu, X., Liu, W., Yang, H., Tang, Q., Flörke, M., Masaki, Y., et al. (2019). Multimodel assessments of human and climate impacts on mean annual streamflow in China. *Hydrology and Earth System Sciences*, *23*(3), 1245–1261.

Liu, X., Tang, Q., Liu, W., Veldkamp, T. I. E., Boulange, J., Liu, J., et al. (2019). A spatially explicit assessment of growing water stress in China from the past to the future. *Earth's Future*, *7*(9), 1027–1043.

Mekonnen, M. M., & Hoekstra, A. Y. (2016). Four billion people facing severe water scarcity. *Science Advances*, *2*(2), e1500323.

Müller Schmied, H., Adam, L., Eisner, S., Fink, G., Flörke, M., Kim, H., et al. (2016). Variations of global and continental water balance components as impacted by climate forcing uncertainty and human water use. *Hydrology and Earth System Sciences*, *20*(7), 2877–2898.

Oki, T., & Kanae, S. (2006). Global hydrological cycles and world water resources. *Science*, *313*(5790), 1068–1072.

Pastor, A. V., Ludwig, F., Biemans, H., Hoff, H., & Kabat, P. (2014). Accounting for environmental flow requirements in global water assessments. *Hydrology and Earth System Sciences*, *18*(12), 5041–5059.

Portmann, F. T., Siebert, S., & Doll, P. (2010). MIRCA2000-Global monthly irrigated and rainfed crop areas around the year 2000: A new high-resolution data set for agricultural and hydrological modeling. *Global Biogeochem Cycles*, *24*, GB1011.

Postel, S. L., Daily, G. C., & Ehrlich, P. R. (1996). Human appropriation of renewable fresh water. *Science*, *271*(5250), 785–788.

Qin, Y., Mueller, N. D., Siebert, S., Jackson, R. B., AghaKouchak, A., Zimmerman, J. B., et al. (2019). Flexibility and intensity of global water use. *Nature Sustainability*, *2*(6), 515–523.

Quinteiro, P., Rafael, S., Villanueva-Rey, P., Ridoutt, B., Lopes, M., Arroja, L., & Dias, A. C. (2018). A characterisation model to address the environmental impact of green water flows for water scarcity footprints. *Science of the Total Environment*, *626*, 1210–1218.

Rockström, J., Falkenmark, M., Karlberg, L., Hoff, H., Rost, S., & Gerten, D. (2009). Future water availability for global food production: The potential of green water for increasing resilience to global change. *Water Resources Research*, *45*(7), W00A12.

Rohwer, J., Gerten, D., & Lucht, W. W. (2007). *Development of functional irrigation types for improved global crop modelling, PIK report No. 104, Tech. Rep. 104, Potsdam Institute for Climate Impact Research*. Germany.

Rost, S., Gerten, D., Bondeau, A., Lucht, W., Rohwer, J., & Schaphoff, S. (2008). Agricultural green and blue water consumption and its influence on the global water system. *Water Resources Research*, *44*(9), W09405.

Savenije, H. H. G. (2000). Water scarcity indicators; the deception of the numbers. *Physics and Chemistry of the Earth. Part B: Hydrology, Oceans and Atmosphere*, *25*(3), 199–204.

Schewe, J., Heinke, J., Gerten, D., Haddeland, I., Arnell, N. W., Clark, D. B., et al. (2014). Multimodel assessment of water scarcity under climate change. *Proceedings of the National Academy of Sciences of the United States of America*, *111*(9), 3245–3250.

Schyns, J. F., Hoekstra, A. Y., & Booij, M. J. (2015). Review and classification of indicators of green water availability and scarcity. *Hydrology and Earth System Sciences*, *19*(11), 4581–4608.

Schyns, J. F., Hoekstra, A. Y., Booij, M. J., Hogeboom, R. J., & Mekonnen, M. M. (2019). Limits to the world's green water resources for food, feed, fiber, timber, and bioenergy. *Proceedings of the National Academy of Sciences of the United States of America*, *116*(11), 4893–4898.

Sen, P. K. (1968). Estimates of the regression coefficient based on Kendall's Tau. *Journal of the American Statistical Association*, *63*(324), 1379–1389.

Sitch, S., Smith, B., Prentice, I. C., Arneth, A., Bondeau, A., Cramer, W., et al. (2003). Evaluation of ecosystem dynamics, plant geography and terrestrial carbon cycling in the LPJ dynamic global vegetation model. *Global Change Biology*, *9*(2), 161–185.

Tuninetti, M., Tamea, S., & Dalin, C. (2019). Water debt indicator reveals where agricultural water use exceeds sustainable levels. *Water Resources Research*, *55*(3), 2464–2477.

Wada, Y., Wisser, D., & Bierkens, M. F. P. (2014). Global modeling of withdrawal, allocation and consumptive use of surface water and groundwater resources. *Earth System Dynamics*, *5*(1), 15–40.

Wang, K. C., & Dickinson, R. E. (2012). A review of global terrestrial evapotranspiration: Observation, modeling, climatology, and climatic variability. *Reviews of Geophysics*, *50*(2), 2011RG000373.

Weedon, G. P., Balsamo, G., Bellouin, N., Gomes, S., Best, M. J., & Viterbo, P. (2014). The WFDEI meteorological forcing data set: WATCH Forcing Data methodology applied to ERA-Interim reanalysis data. *Water Resources Research*, *50*(9), 7505–7514.

Xu, H., & Wu, M. (2018). A first estimation of county-based green water availability and its implications for agriculture and bioenergy production in the United States. *Water*, *10*(2), 148.

Yano, S., Hanasaki, N., Itsubo, N., & Oki, T. (2016). Potential impacts of food production on freshwater availability considering water sources. *Water*, *8*(4), 163.

Zhu, W., Jia, S., Devineni, N., Lv, A., & Lall, U. (2019). Evaluating China's water security for food production: The role of rainfall and irrigation. *Geophysical Research Letters*, *46*(20), 11155–11166.